ORIGINAL PAPER

Mesoporous silica xerogel modified with bridged ionic silsesquioxane used to immobilize copper tetrasulfonated phthalocyanine applied to electrochemical determination of dopamine

Monique Deon · Elisangela Muncinelli Caldas · Danielle Santos da Rosa ·
Eliana Weber de Menezes · Silvio Luis Pereira Dias · Marcelo Barbalho Pereira ·
Tania Maria Haas Costa · Leliz Ticona Arenas · Edilson Valmir Benvenutti

Abstract Silica xerogel was modified with an ionic silsesquioxane containing the cationic 1,4-diazoniabicyclo[2.2.2]octane bridged group and it was used as matrix for immobilization of copper tetrasulfonated phthalocyanine, resulting in Si/Db/CuTsPc material. This material was characterized by ultraviolet-visible and infrared spectroscopy, elemental and thermogravimetric analyses, nitrogen adsorption-desorption isotherms, and scanning electron microscopy. The Si/Db/CuTsPc material was used to develop a carbon paste electrode for dopamine determination. The electrochemical behavior of dopamine was evaluated by cyclic voltammetry and chronoamperometry. The optimal experimental conditions were determined (pH=4.5 and oxygen atmosphere) using a 0.1 mol L^{-1} phosphate buffer solution. The carbon paste electrode modified with the Si/Db/CuTsPc material shows a linear response for current intensity with the dopamine concentration in the range of 0.010 to 0.107 mmol L^{-1}. The detection limit was 0.42 μmol L^{-1}, and the sensitivity was 7.15 μA (mmol L^{-1})$^{-1}$, making the system promising to be applied as electrochemical sensor for dopamine.

M. Deon · E. M. Caldas · D. S. da Rosa · E. W. de Menezes ·
S. L. P. Dias · T. M. H. Costa · L. T. Arenas · E. V. Benvenutti (✉)
LSS – Instituto de Química, UFRGS, CP 15003, CEP
91501-970 Porto Alegre, RS, Brazil
e-mail: benvenutti@ufrgs.br

M. B. Pereira
LLO – Instituto de Física, UFRGS, CP 15015, CEP 91501-970 Porto
Alegre, RS, Brazil

Introduction

Dopamine (DA) is an important neurotransmitter in the mammalian central nervous system. The dopaminergic system is strictly related to diseases such as Parkinson, Alzheimer, hyperactivity, schizophrenia, depression, substance abuse, and eating disorders [1]. Therefore, the determination of DA in drugs and bodily fluids is very important. Its basal concentration is in the range of 0.01–1 μmol L^{-1} [2, 3]. The most used detection methods for dopamine include capillary electrophoresis [4], colorimetric [5], high performance liquid chromatography [6], and fluorescence sensors [7], among others. Considering that DA can be easily oxidized, electrochemical methods have been studied in the last 20 years, highlighted for the last 10 years, when the publications arise exponentially.

Electrochemical sensors present some advantages when compared with the classical analytical methods, such as fast response, low cost equipment and analysis, easy sample handling, and excellent sensitivity [8–11]. These devices usually need the addition of modifier species to improve the performance of the electrode, upgrading their sensitivity and selectivity. It was reported, for DA determination, the use of modified metal electrodes such as gold and platinum [12, 13], modified glassy carbon electrodes [14, 15] and, in some cases, the use of nanostructures as metal nanoparticles and carbon nanotubes [16, 17]. Furthermore, modified carbon

paste electrodes (CPE) are also largely employed in the development of electrochemical sensors [18–20]. The advantages of using CPE are the low cost and easy to prepare; they also offer a wide potential window with low background current [21]. In addition, CPE can be obtained using several chemically modified porous materials [22].

Mesoporous silica materials (2 a 50 nm) [23] are excellent supports for electroactive species, since they present the properties of the rigid structure of silica, with large surface area and pore volumes, allowing the immobilization of species inside the porous structure, providing fast mass transport [24–26]. The organofunctionalization of silica materials can be performed using grafting reactions, due to the reactive silanol groups available on the surface, resulting in a solid with the mechanical and thermal stability of silica matrix and the chemical reactivity of organic groups [27].

Ionic silsesquioxanes are hybrid materials obtained from the gelation of ionic organosilanes [28, 29]. They are water-soluble and, additionally, they have silanol groups that provide the ability to be deposited on inorganic matrix surfaces [30, 31]. The ionic silsesquioxanes provide an increase in the electroactive area of the electrode [32, 33]. Moreover, the presence of ionic groups allows their use as anion exchanger materials [22, 34, 35]. Therefore, it is possible the insertion of anionic electroactive species, which can improve the electrochemical characteristics of the electrode [29, 36]. Among the anionic electroactive species, the metallophthalocyanines are well known for their excellent catalytic properties for several reactions [37], with high chemical and thermal stability [38]. They have been used in electrochemical sensors to detect analytes such as serotonin [39], dissolved oxygen [40], nitric oxide [41], cysteine [42], nitrite [43], oxalic acid [44], ascorbic acid [45, 46], uric acid [46], phenols [47], and more specifically the dopamine [36, 45, 46, 48, 49].

In this work, an organofunctionalized silica containing the bridged 1,4-diazoniabicyclo[2, 2, 2]octane group was obtained. Due to the presence of ionic groups, this material was used as support for the immobilization of copper tetrasulfonated phthalocyanine by ion-exchange process. The resulting material was characterized by spectroscopy in the infrared and UV-Vis region, thermogravimetric, elemental, and textural analyses. A carbon paste electrode modified with this material was prepared and it was used for dopamine determination by cyclic voltammetry and chronoamperometry.

Experimental

Chemicals

Ionic silsesquioxane which contains the 1,4-diazoniabicyclo[2.2.2]octane chloride group was prepared according to previous report [50]. Other reagents

used were as follows: tetraethyl orthosilicate (TEOS) (Aldrich, 98 %), methanol (Merck, 99.8 %), ethanol (Merck, 99.9 %), copper phthalocyanine-3,4′,4″,4‴-tetrasulfonic acid tetrasodium salt (CuTsPc) (Aldrich, 85 %), graphite powder (Aldrich, 99.99 %), hydrofluoric acid (HF) (Merck), and dopamine hydrochloride (Sigma, 98 %), all analytical grade. Phosphate buffer solution (PBS, 0.1 mol L^{-1}, pH 7.0) was prepared from NaH_2PO_4 and Na_2HPO_4. Hydrochloric acid (HCl) (Merck) was used for pH control. Mineral oil was used for the electrode manufacture. All the solutions were prepared in distilled water.

Materials preparation

In the synthesis of Silica xerogel matrix, 5 mL of TEOS was added into a beaker containing 10 mL of methanol. Then, 3 mL of methanol, 3 mL of distilled water, and 3 drops of HF were added in sequence. The mixture was stirred and stored for gelation at ambient conditions. After 15 days, the xerogel monolith was powdered, washed with water and ethanol, and vacuum-dried at 80 °C for 2 h.

The immobilization of ionic silsesquioxane onto silica surface was performed using 0.55 g of silsesquioxane in 40 mL of water. This solution was added to 1.50 g of silica and kept in shaking for 8 h and rest overnight. The supernatant was separated, and the solid was vacuum-dried at 80 °C for 1 h, then it was washed several times with water, ethanol and dried again under same conditions for 2 h. This material was hereafter called Si/Db, where Db specifies the cationic 1,4-diazoniabicyclo[2.2.2]octane group of silsesquioxane.

CuTsPc was immobilized using a 0.25 mg mL^{-1} solution in distilled water. The Si/Db was immersed in the CuTsPc solution and kept under shaking for 3 days, with rest overnight. The CuTsPc solution was changed approximately each 3 h. After the immobilization process, the solid was washed with water and vacuum-dried at 80 °C for 1 h. The resultant material was hereafter called Si/Db/CuTsPc.

Characterization of Silica, Si/Db, and Si/Db/CuTsPc materials

The Infrared analysis was performed using an IR cell that allows obtaining spectra of samples heat-treated in vacuum, without air exposition. The IR cell was described elsewhere in detail [51]. Self-supporting disks of the materials, with a diameter of 2.5 cm, weighing *ca.* 100 mg were prepared. The disks were heated at 130 °C, under vacuum (10^{-2} Torr) for 1 h. The spectra were obtained at room temperature, using a Shimadzu FTIR, Prestigie 21, with a resolution of 4 cm^{-1} and 100 cumulative scans.

The elemental analysis of the organic groups was carried out in a CHN Perkin Elmer M CHNS/O Analyzer, model 2400.

The thermogravimetric analysis of the materials was performed under nitrogen flow on a Shimadzu Instrument model TGA-50, with a heating rate of 10 °C min^{-1}, from room temperature up to 700 °C.

The UV-Vis analysis for CuTsPc aqueous solution was performed using a spectrophotometer Agilent CARY 50 Conc. On the other hand, for the Si/Db/CuTsPc powder material, the absorbance was determinate by diffuse reflectance, using a double beam spectrophotometer Agilent CARY 5000 with integrate sphere accessory. To determine the absorbance bands of the material, a sample holder with a fused silica window was fulfilled with the powder forming a thicker layer of the material (semi-infinite medium).

The N$_2$ adsorption-desorption isotherms were determined at liquid nitrogen boiling point, using a Tristar 3020 Kr Micromeritics equipment. The samples were previously degassed at 120 °C under vacuum, for 12 h. The specific surface areas were determined by the BET (Brunauer, Emmett and Teller) multipoint technique, and the pore size distribution was obtained by using the BJH (Barret, Joyner and Halenda) method [52].

Scanning Electron Microscopy (SEM) images were obtained using a scanning electron microscope, model JSM 5800 LV, JEOL, connected to a secondary electron detector with energy dispersive spectroscopy (EDS). The materials were dispersed on a double side conducting tape on an aluminum support and coated with a thin film of platinum using a Balted SCD 050 Sputter Coater apparatus. The images were obtained with a magnification of ×20,000 operating at an accelerating voltage of 15 kV. EDS analysis was obtained from different parts of the Si/Db/CuTsPc.

Electrochemical measurements

Carbon paste electrode (CPE) was prepared by mixing 10 mg of Si/Db/CuTsPc and 10 mg of graphite in agate mortar, followed by the addition of 3.3 mg of mineral oil. The resultant paste was pressed against a platinum disk in the extremity of a glass tube. The electric contact was made with a copper wire.

Electrochemical measurements were carried out on IviumStat potentiostat/galvanostat apparatus using an electrochemical cell with three electrodes. The electrodes were a saturated calomel electrode (SCE) and a platinum wire as reference and auxiliary electrodes, respectively, and the previously prepared CPE as working electrode. All the measures were made at room temperature.

Results and discussion

Synthesis and characterization of the materials

The synthesis of the ionic silsesquioxane which contains the 1,4-diazoniabicyclo[2.2.2]octane chloride group (SiDbCl$_2$) was already reported [50] and a representation of its structure is shown in Supplementary material.

Infrared spectra of Silica, Si/Db, and Si/Db/CuTsPc previously heated up to 130 °C under vacuum, are presented in the Fig. 1. The silica xerogel overtone bands can be observed in the range from 2000 to 1600 cm^{-1}, highlighting the 1875 cm^{-1} band [53]. The broadband centered at 3300 cm^{-1} is due to the O-H stretching frequency of the silanols. The presence of a sharp peak at 3736 cm^{-1} is observed in the Silica material, indicating the presence of free silanol groups (SiOH) [54]. This band was significantly reduced after the silsesquioxane immobilization (Si/Db and Si/Db/CuTsPc spectra), indicating the silsesquioxane was grafted onto the silica surface by the silanol crosslinking reactions [55]. The organic moiety in Si/Db and Si/Db/CuTsPc materials can be identified by the band at 1466 cm^{-1}, assigned to CH$_2$ bending [56, 57] and also the bands between 3000 and 2900 cm^{-1} due to C-H stretching. The presence of these organic bands, even after heat treatment at 130 °C, in vacuum, confirms the silsesquioxane is strongly bonded to the silica surface [33, 51, 55].

The presence of phthalocyanine was not observed by the infrared analysis. In this case, the UV-Vis spectroscopy provides more conclusive information. Figure 2a shows the UV-Vis absorption spectrum of CuTsPc aqueous solution. It is possible to observe the presence of two absorption bands in the Q-band region of the phthalocyanine. The first band has a maximum at 631 nm and the second one appears at *ca.*
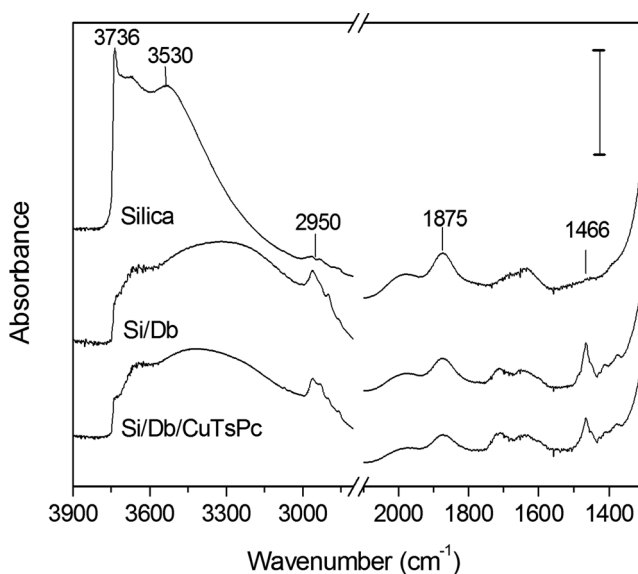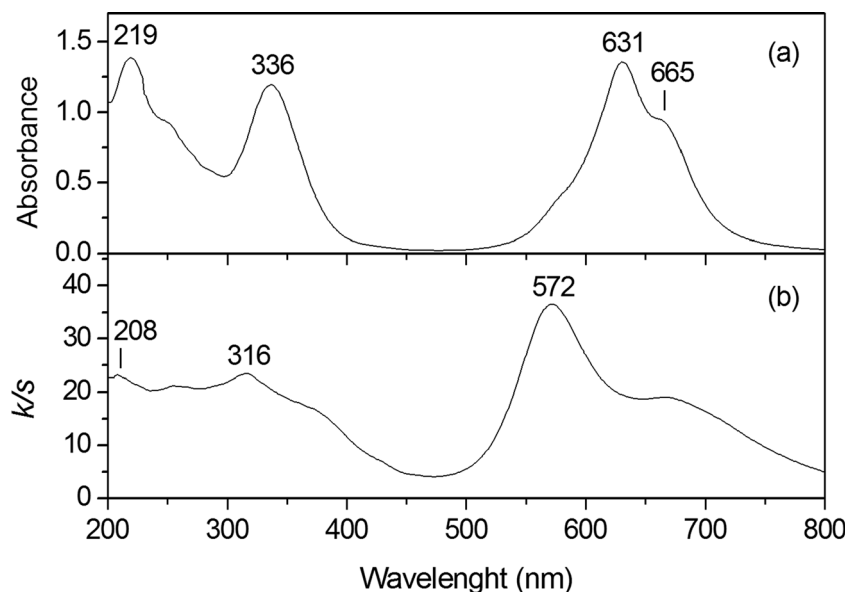

Fig. 1 Absorbance infrared spectra obtained at room temperature, after heat treatment at 130 °C for 1 h in vacuum. The bar value is 0.4

Fig. 2 Absorbance spectra in the UV-Vis region (**a**) CuTsPc (aqueous) and (**b**) Si/Db/CuTsPc (solid)

665 nm, which are related to the dimeric and monomeric phthalocyanine species, respectively [58, 59]. The band at 631 nm is more intense than that at 665 nm, indicating that the phthalocyanine in solution preferably takes the form of dimeric species. The presence of absorption bands in the Soret-band region, between 219 and 336 nm, were attributed to electronic transitions of $\pi \rightarrow \pi^*$ type of the macrocyclic ring of phthalocyanine [59].

Figure 2b shows the UV-Vis absorbance spectrum of the Si/Db/CuTsPc. In this case, it can be observed a broadening of the bands assigned to dimeric and monomeric phthalocyanine species [38], if compared to the absorption spectrum of the CuTsPc aqueous solution (Fig. 2a). It was also observed that the peak related to the dimeric species was shifted from 631 to 572 nm. These facts can be assigned to the confinement of the CuTsPc inside of the pores, leading to an increase in the intermolecular interaction [36, 38] or to the distortion of the D_{4h} symmetry [49].

The weight loss values obtained from the TGA analysis of Silica, Si/Db, and Si/Db/CuTsPc are presented in Table 1, along with the elemental analysis, which was estimated by CHN and EDS. The weight loss from room temperature to 150 °C was assigned to water desorption. In the range from 150 to 600 °C, it was observed a significant weight loss for Si/Db and Si/Db/CuTsPc, which was attributed to decomposition of organics and dehydroxylation reactions of the silanol groups [54]. For Silica, this weight loss was due to only dehydroxylation reactions. The TGA curves are shown in Supplementary material.

For the Si/Db, the value of 3.88 mmol of carbon per gram of material was found by CHN elemental analysis, corresponding to 0.29 mmol of cationic Db group per gram of material. This result is in agreement with the nitrogen analysis for Si/Db, where it was found the value of 0.51 mmol of nitrogen per gram of material, corresponding to 0.25 mmol of cationic Db group per gram of material. After the insertion of phthalocyanine, richer in nitrogen content than silsesquioxane chain, there was a reduction of near 30 % in the carbon amount and a slight increase of 4 % in nitrogen (Si/Db/CuTsPc). This trend can be interpreted taking into account the leaching of the ionic silsesquioxane during the phthalocyanine immobilization process, which is performed in aqueous

Table 1 Elemental and thermogravimetric analysis and textural data

Material	Elemental analyses			TGA analysis	Textural analysis	
	C^a	N^a	Cu^b	Weight loss% (150–600 °C)	$S_{BET}/\pm 10 \ m^2 \ g^{-1}$	$V_p/\pm 0.01 \ cm^3 \ g^{-1}$
Silica	0.43	0.01	–	2.5	381	1.03
Si/Db	3.88	0.51	–	5.8	311	0.87
Si/Db/CuTsPc	2.78	0.53	0.14	5.6	286	0.89

[a] mmol of element per gram of material

[b] mmol of copper per gram of material. Obtained from EDS analysis (±0.03)

S_{BET} specific surface area, V_p pore volume

solution during 72 h. This leaching was already reported for ionic silsesquioxanes immobilized on silica surfaces [57]. This hypothesis was also confirmed by thermogravimetric analysis, where it was observed a slight mass reduction, in the range of temperature between 150 and 600 °C, after the phthalocyanine insertion. The copper EDS analysis confirmed the presence of phthalocyanine, showing a copper amount of 0.14 mmol per gram of material.

Textural characteristics of the materials were investigated using the N_2 adsorption-desorption isotherms, obtained at nitrogen boiling point temperature. The N_2 isotherms and the BJH pore size distribution are shown in Fig. 3. The isotherms were classified as type IV, typical of mesoporous materials [52], confirmed by BJH pore size distribution curves. All materials present a similar profile with pore size distribution ranging from 7 to 12 nm. Additionally, it was obtained significant values for BET specific surface area and pore volume, which are shown in Table 1. The variations in BET surface area and pore volume observed after the silica matrix modification are compatible with the immobilization of the species inside of the pores. These textural characteristics such as pore size and surface area allowed the modification of the silica surface with silsesquioxane macromolecules and also the immobilization of large electroactive species, in this case, phthalocyanine, as confirmed by infrared and UV-Vis spectroscopy and also elemental analysis. Furthermore, the large porous structure allows the access of analytes to the phthalocyanine active sites.

In a general way, the surface modification by large species, such as phthalocyanine, leads to a decrease in the pore size. In the present work, it was observed an opposite effect, i.e., after the phthalocyanine insertion, the maximum pore distribution shifts in about 1 nm to higher values. This result is consistent since it was observed for repeated samples. This trend was interpreted taking into account the ionic silsesquioxane leaching process that occurs during the phthalocyanine

immobilization, discussed above, which can be followed by an erosive process of silica matrix pore wall.

Silica, Si/Db, and Si/Db/CuTsPc were submitted to SEM analysis and typical images are presented in Supplementary material. It is possible to observe comparable images for all materials, indicating the supposed erosive process that occurs inside pores does not take place in the micrometric level. Furthermore, the immobilization process by shaking is softer than mechanical or magnetic stirring, which could produce grooves on silica surface [60].

Electrochemical characterization

In order to study the electrochemical performance of the Si/Db/CuTsPc material in the redox process of dopamine, carbon paste electrodes (CPE) were prepared and used in cyclic voltammetry experiments. Figure 4 shows the voltammograms in the absence and in the presence of dopamine for Si/Db and Si/Db/CuTsPc CPEs. It is possible to observe that both materials present electrochemical response for dopamine, Si/Db/CuTsPc CPE shows lower peak potentials and higher current peak intensity than Si/Db CPE. Aiming to find the optimum conditions for dopamine detection, pH effects on the electrochemical behavior of dopamine were studied, and the results are shown in Fig. 5.

It can be seen that the redox process of dopamine was favored in low pH, since the peak current intensity was higher, with lower peak-to-peak separation. In acid pH, the species is mostly in the protonated form (DAH$^+$) [36, 61]. In this way, the DAH$^+$ is oxidized to dopaminoquinone in a two-proton and two-electron mechanism [62, 63] as represented in Fig. 6. Moreover, the sulfonic groups of phthalocyanine are expected to be anionic in low pH [38, 64], since the pK_a of sulfonic groups in TsPc is considered as near to the benzene sulfonic acid (pK_a=0.7) [64, 65]. However, it was reported that the pK_a value of TsPc is slightly higher when there is a metal
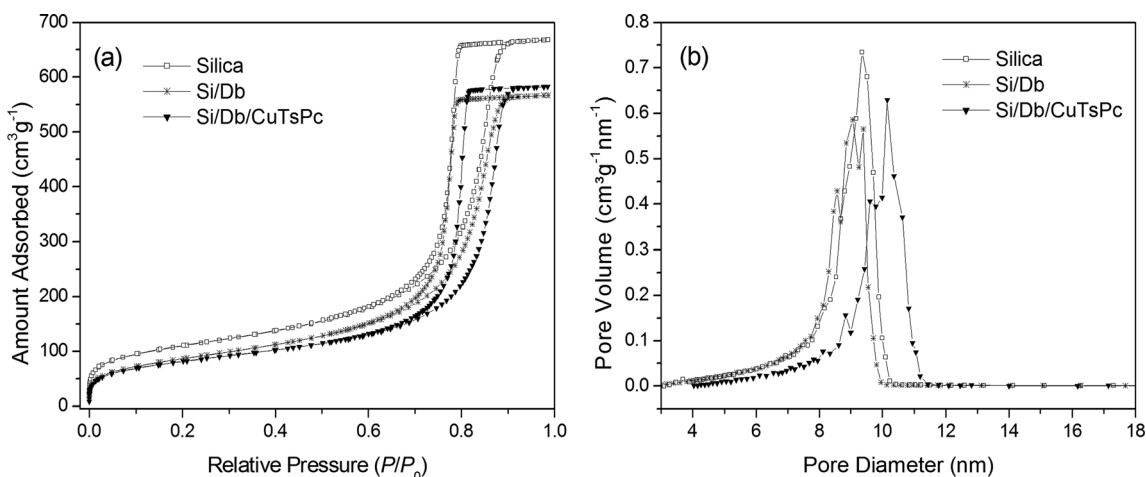

Fig. 3 Textural analysis (**a**) N_2 adsorption-desorption isotherms and (**b**) BJH pore size distributions
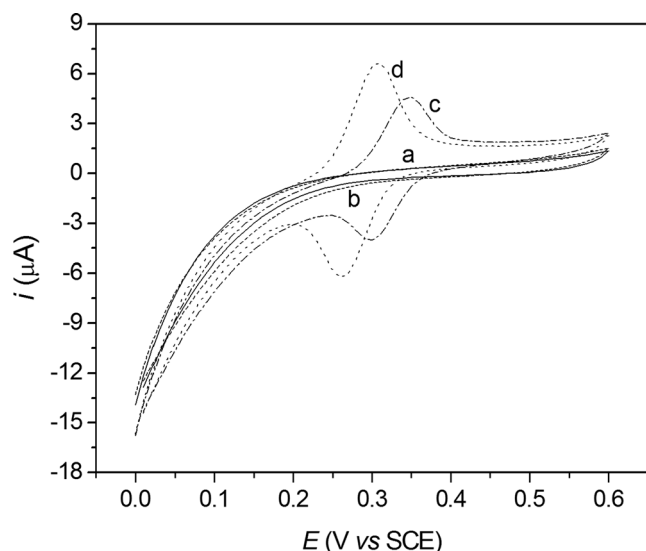
Fig. 4 Cyclic voltammograms of Si/Db CPE (**a**) and Si/Db/CuTsPc CPE (**b**) in the absence of dopamine; and Si/Db CPE (**c**) and Si/Db/CuTsPc CPE (**d**) in the presence of dopamine, 0.0910 mmol L^{-1}. Scan rate= 20 mV s^{-1}

coordinated to the TsPc, which is due to small back-bonding capability between the metal center and the ligands [64]. Thus, considering the anionic form of sulfonic groups in low pH, the DAH$^+$ is electrostatically attracted to the surface of electrode [36, 66–68] as shown in Fig. 6. In this way, it was proposed an electrostatic adsorption mechanism for dopamine, which promotes the electrocatalysis in the redox process of dopamine, justifying the high peak current intensities and the lower potentials for Si/Db/CuTsPc CPE, when compared to Si/Db
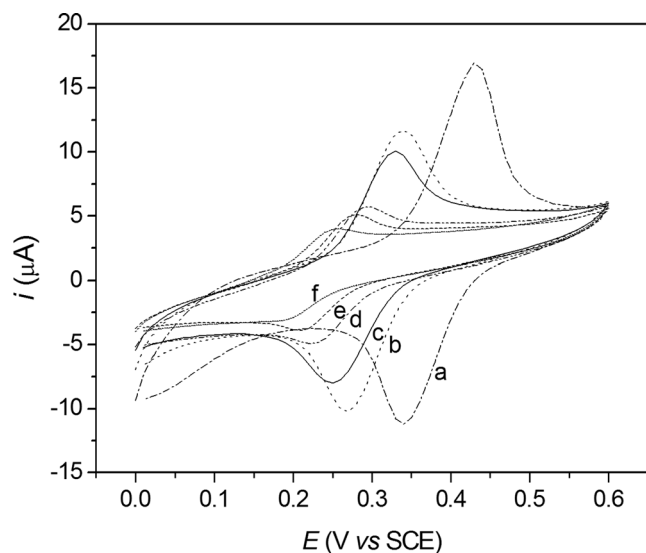

Fig. 5 Cyclic voltammograms of the Si/Db/CuTsPc CPE in the presence of 0.0910 mmol L^{-1} of dopamine in PBS 0.1 mol L^{-1} at pH (**a**) 3.0, (**b**) 4.0, (**c**) 4.5, (**d**) 5.0, (**e**) 5.5, and (**f**) 6.0. Scan rate=20 mV s^{-1}

CPE, already shown in Fig. 4. Additionally, metallophthalocyanines present electrocatalytic properties due to the synergic effect of metallic center and delocalized π electrons in the structure, enabling fast electron transfer [69, 70].

However, in the present work, at pH lower than 4.0, the dopamine remains adsorbed on the CPE surface, hampering the electrode reuse. Therefore, the pH chosen for measures was 4.5, where the dopamine shows well defined current peaks and the CPE can be reused.

The peak potentials and intensities versus pH are presented in the Supplementary material. From the plots of pH as function of E_p values, two curves were obtained: one for the anodic peak and the second one for cathodic peak potentials. Both present linear behavior, with R^a=−0.9789 and R^c=−0.9903 (where R^a and R^c are the linear correlation coefficient for anodic and cathodic peak potential, respectively) and the equations are $E_{pa}(V)= 0.58\ (\pm0.03)-0.056\ (\pm0.006)\ pH$ and $E_{pc}(V)= 0.48\ (\pm0.01)-0.051\ (\pm0.004)\ pH$. The slope values 0.056 and 0.051 are very close to Nernst theoretical value of 0.059 V pH^{-1} at 25 °C. According to the equations $0.059x/n= 0.056$ and $0.059x/n= 0.051$, where n is the number of transferred electron and x is the number of participating hydrogen ions, the ratio between hydrogen ions and electrons is 1, which confirms the already defined two-protons and two-electrons mechanism [71, 72].

The influence of the atmosphere in the redox process using Si/Db/CuTsPc CPE was studied. It was observed that the oxygen atmosphere shows better response in current intensity, improving the sensibility. Thus, this atmosphere was chosen for the measures. The results are shown as Supplementary material.

Figure 7 shows the cyclic voltammograms of the electrode at different scan rates, from 5 to 200 mV s^{-1}. The potentials and peak currents are dependent of the scan rate. The peak current increase linearly with the scan rate (Inset Figure), with R^a=0.9983 and R^c=− 0.9978. The linear regression equations are $I_{pa}(\mu A)=2.1\ (\pm0.3)+0.188\ (\pm0.003)\ v(mV\ s^{-1})$ and $I_{pc}(\mu A)=-1.8\ (\pm0.4)-0.198\ (\pm0.004)\ v(mV\ s^{-1})$. These results indicate a redox process, on the electrode surface, controlled by adsorption [73] confirming the mechanism proposed above. Also, the E_{pa} shifted to higher values, and the E_{pc} shifted to lower values with the increase of the scan rate. A linear correlation was observed for scan rate and ΔE_p (Supplementary material), with $R= 0.9843$, suggesting a quasi-reversible process.

According to Laviron theories [74], when $n\Delta E_p > 200$ mV, where n is the number of electrons involved, the charge transfer coefficient (α) can be calculated from the correlation between E_p and log v, which in high scan rates, presents a linear behavior. In this way, the following equations are given
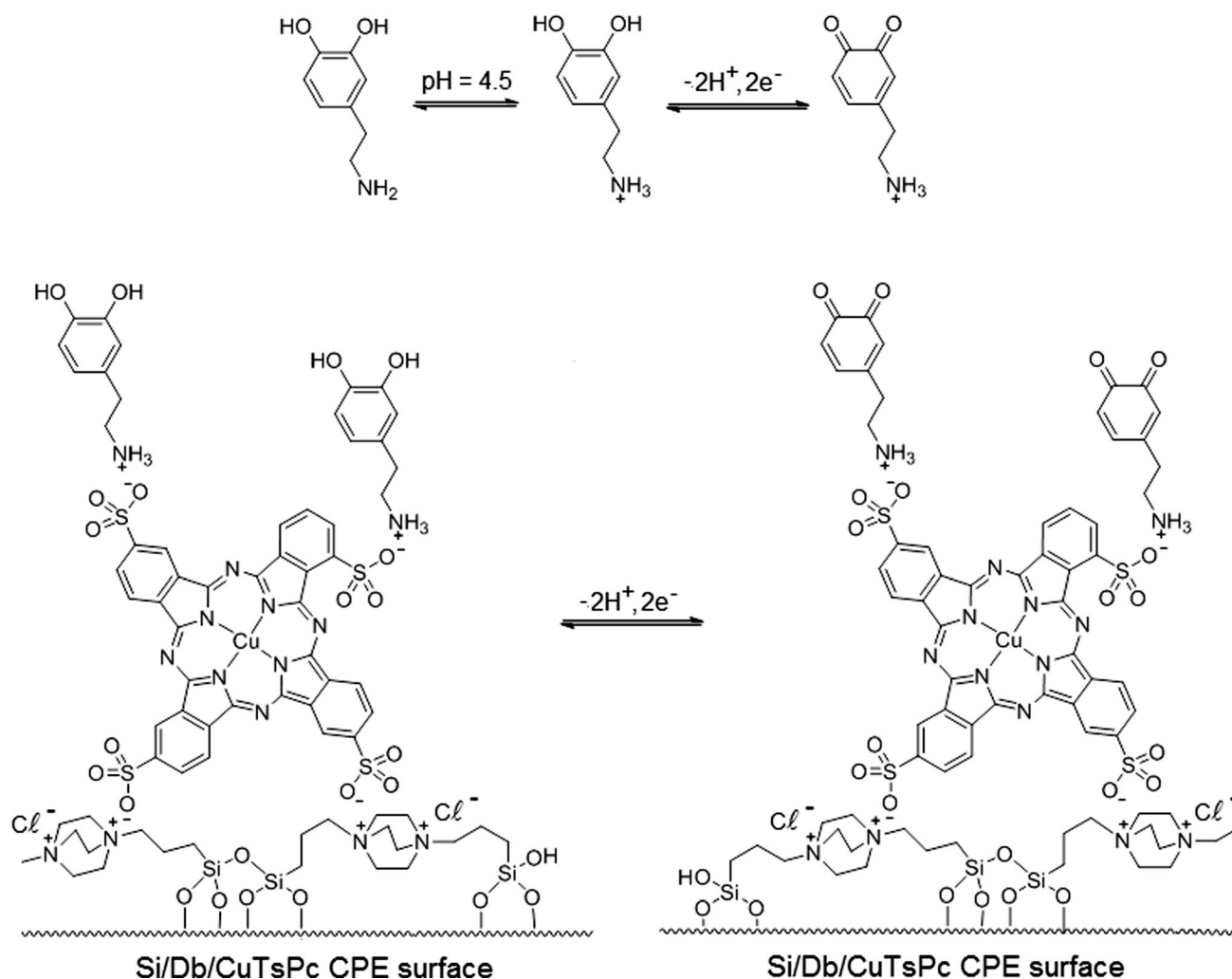
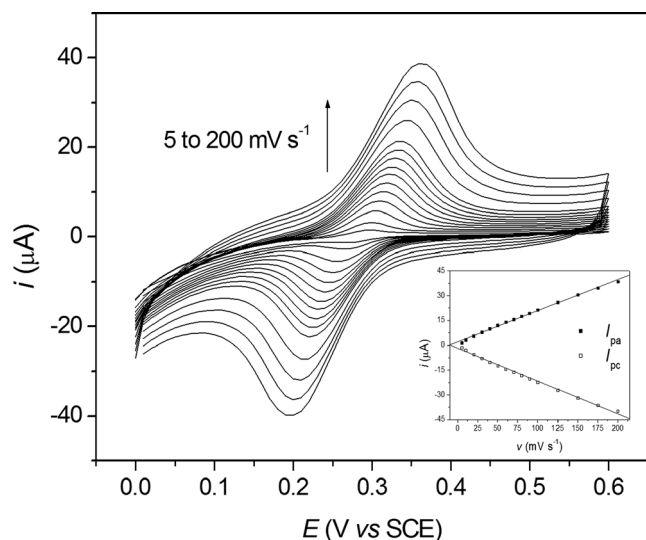**Fig. 6** Representation of dopamine oxidation mechanism on electrode surface

Fig. 7 Cyclic voltammograms of CPE containing Si/Db/CuTsPc in the presence of 0.0910 mmol L^{-1}, PBS 0.1 mol L^{-1}, pH 4.5, in the scan rate range of 5 to 200 mV s^{-1}. *Inset figure*, correlation between scan rate and I_{pa} and I_{pc}

as follows:

$$E_{pa} = E_c^{\ominus} + \left[2.3RT \Big/ (1-\alpha)nF\right] \log v \qquad (1)$$

$$E_{pc} = E_c^{\ominus} - \left[2.3RT \Big/ \alpha nF\right] \log v \qquad (2)$$

where $E_c^{\ominus}$ is the formal potential estimated from [($E_{pa}+E_{pc}$)/2], R is the ideal-gas constant (8.314 J K^{-1} mol^{-1}), T is the temperature (298 K), and F is the Faraday constant (96.4885 10^3 C mol^{-1}).

The correlation between log v and E_p are shown in the Supplementary material. For the CPE containing Si/Db/CuTsPc, when $v > 100$ mV s^{-1}, a linear behavior is observed, and at $v = 100$ mV s^{-1}, the value of $n\Delta E_p$ is 234 mV, obeying the Laviron theory requirements. The linear regression equations were $E_{pa} = 0.425 (\pm 0.002) + 0.090 (\pm 0.003) \log v$ with $R^a = 0.9969$ and $E_{pc} = 0.136 (\pm 0.002) - 0.086 (\pm 0.003) \log v$ with $R^c = -0.9964$. The α value 0.507 was calculated as the mean of the values obtained from anodic and cathodic peaks.
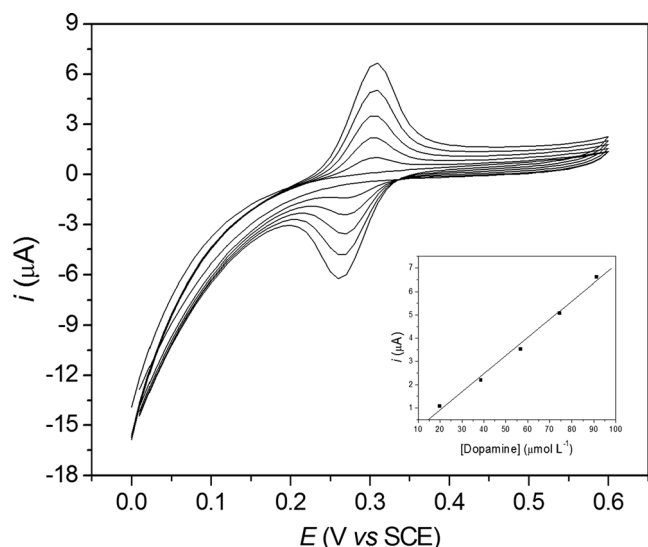
Fig. 8 Cyclic voltammograms of sequential additions, 0.4 μmol of dopamine in PBS 0.1 mol L^{-1}, pH 4.5, under oxygen atmosphere, scan rate=20 mV s^{-1}. *Inset figure*, correlation between dopamine concentration and anodic peak current

Also, electron transfer rate constant (k_s) was calculated according to Eq. 3, where the obtained value was 0.398 s^{-1}.

$$\log k_s = \alpha \log(1-\alpha) + (1-\alpha)\log\alpha - \log\left(RT/nFv\right) - \alpha(1-\alpha)nF\Delta E_p/2.3RT \tag{3}$$

Sequential additions of dopamine, using cyclic voltammetry, were performed, and the results are shown in Fig. 8. The cyclic voltammogram of Si/Db/CuTsPc CPE in the presence of 0.0910 mmol L^{-1} dopamine showed a pair of well-defined and nearly symmetric redox peaks. The ratio of the anodic

peak current and cathodic peak current is I_{pa}/I_{pc}=1.073 and ΔE_p=0.048 V. These characteristics are typical quasi-reversible process. Additionally, it is possible to notice a linear correlation between dopamine concentration and the peak current (R=0.9964) in the range of 0.0196 to 0.0910 mmol L^{-1}.

To obtain a better evaluation of the linear response, detection limit, and sensitivity, chronoamperometric measurements were performed, and the results are shown in Fig. 9. The studied linear range was 0.010 to 0.107 mmol L^{-1}. The linear regression was expressed by the following equation: $I(\mu A) = -0.015 \ (\pm 0.007) + 7.15 \times 10^{-3} \ (\pm 9 \times 10^{-5})$ [dopamine](μmol L^{-1}) and the R was 0.9991. The sensitivity was obtained by the slope of the curve with the value of 7.15 μA (mmol L^{-1})$^{-1}$. The detection limit was calculated by the ratio ($3 \times SD_b$/slope), where SD_b was the standard deviation of blank measurements (n=10), and the obtained value was 0.42 μmol L^{-1}.

The performance of Si/Db/CuTsPc CPE for dopamine electrooxidation was compared with different electrodes already reported, and a detailed comparison is presented in Table 2. It was observed that the Si/Db/CuTsPc CPE presents a better performance than most of the reported systems. It is important to emphasize the electrodes that present lower detection limits contain nanostructures such as carbon nanotubes [16, 17, 66], graphene [20], and metal nanoparticles [8, 62] that improve electrocatalytic response, while the Si/Db/CuTsPc CPE is a simpler system, even so it shows a nonspecific results when in the presence of interferents as ascorbic and uric acids. The reproducibility of the dopamine sensor was investigated by recording cyclic voltammograms of Si/Db/CuTsPc CPE by detecting 0.091 mmol L^{-1} of dopamine at five independently electrodes prepared, and relative standard deviation was about 8 %. These results show the potentiality of the Si/Db/CuTsPc CPE for the application as electrochemical sensor of dopamine.
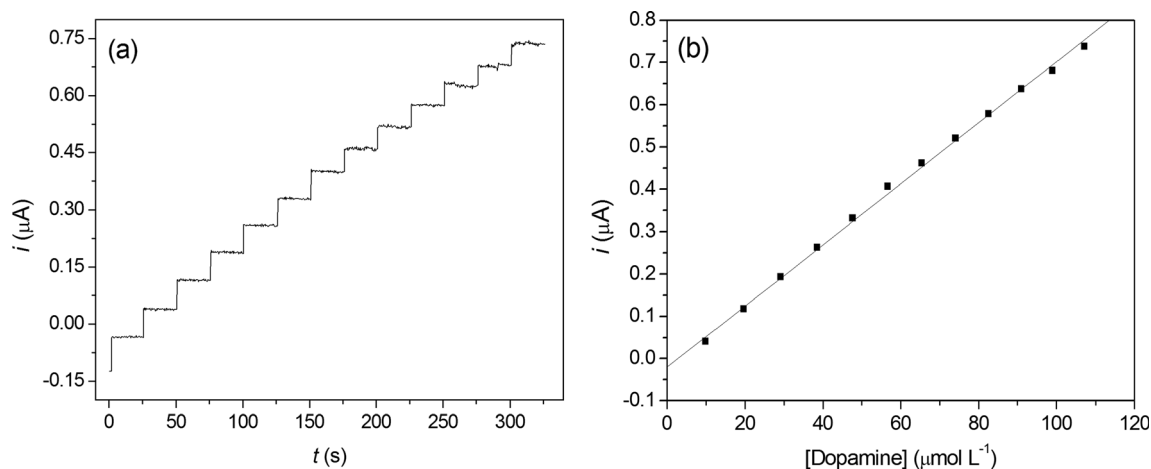

Fig. 9 Chronoamperometric results. **a** Amperometric response of Si/Db/CuTsPc CPE with sequence additions of 0.2 μmol of dopamine in E=+0.33 V vs SCE in PBS 0.1 mol L^{-1}, pH 4.5, under oxygen atmosphere. **b** Calibration curve for the respective electrode

Table 2 Comparative performance of different electrodes for dopamine determination

Electrode	Linear range (μM)	Detection limit (μM)	Reference
ERGO/GCE [a]	0.5 to 60	0.5	[2]
AuNPs@MIPs [b]	0.02 to 0.54	0.0078	[8]
Qu–TCA–MUA/Au [c]	30 to 300	1	[12]
Pt/PEDOT/PDA [d]	1.5 to 50	0.65	[13]
poly(caffeic acid)-modified electrode [e]	1 to 40	0.4	[14]
RuOx–Nf–GC [f]	50 to 1100	5	[15]
PABS MWNT/GCE [g]	9 to 48	0.21	[16]
MB-MWNTs/GCE [h]	0.4 to 10	0.2	[17]
HBNBH-MTNCPE [i]	8.0 to 1400	0.84	[19]
GR/CS/CPE [j]	0.2 to 100	0.0982	[20]
SiPy$^+$Cl$^-$/CuTsPc [k]	49 to 910	10	[36]
FeTSPc–CPE [l]	1.0 to 15	1	[39]
SiO$_2$/C/CuPc [m]	10 to 140	0.6	[49]
ITO-(Ch/NiTsPc)$_n$ [n]	5.0 to 150	48	[58]
Fe$_3$O$_4$-NH$_2$@GS/GCE [o]	0.2 to 38	0.126	[62]
Gr/(PDDA–[PSS-MWCNTs])$_5$ [p]	50 to 350	0.15	[66]
ITO/SiPy$^+$Cl$^-$/NiTsPc [q]	10 to 99	16.8	[67]
IL-CPE [r]	1.0 to 800	0.7	[72]
IL–G/GCE [s]	1 to 400	0.679	[75]
AuNPs@PANI [t]	10 to 1700	5	[76]
Tyrosinase–SWNT–Ppy [u]	5 to 50	5	[77]
GEF/CFE [v]	0.7 to 45.21	0.5	[78]
ITO/ABTS-CNT-Nafion [w]	1.87 to 20.00	1.75	[79]
Si/Db/CuTsPc CPE	9.9 to 107.1	0.42	This work

[a] Electrochemically reduced graphene oxide (ERGO) film-modified glassy carbon electrode (GCE)

[b] Gold nanoparticles (AuNPs) doped molecularly imprinted polymers (MIPs)

[c] Quercetin(Qu)–thioglycolic acid(TCA)–11-mercaptoundecanoic acid(MUA)-modified gold electrode (Au)

[d] Platinum electrode (Pt) modified with a hybrid film of poly(3.4-ethyl-enedioxythiophene)/polydopamine (PEDOT/PDA)

[e] Poly(caffeic acid)-modified glassy carbon electrode

[f] Ruthenium oxide (RuOx) onto Nafion-coated glassy carbon (GC) electrode

[g] Multiwalled carbon nanotubes (MWNT)-modified glassy carbon electrode (GCE) coated with poly (orthanilic acid) (PABS) film

[h] Glassy carbon electrode (GCE) modified with nanocomposite prepared through the adsorption of methylene blue (MB) onto multi-walled carbon nanotubes (MWCNTs)

[i] 2,2′-[1,7-hepthandiylbis (nitriloethylidyne)]-bis-hydroquinone (HBNBH) and TiO$_2$ nanoparticle-based carbon paste electrode (MTNCPE)

[j] Graphene–chitosan (GR-CS) nanocomposite-modified carbon paste electrode (CPE)

[k] Propylpyridiniumsilsesquioxane chloride polymer (SiPy$^+$ Cl$^-$) and copper tetrasulfonated phtahlocyanine (CuTsPc) deposited on fluor tin oxide-covered glass substrates (FTO) using layer-by-layer technique

[l] Carbon paste electrode (CPE) containing iron(II) tetrasulfophthalocyanine ([FeTSPc]$^{4-}$)

[m] Copper(II)phtahlocyanine (CuPc) generated *in situ* in the pores of a matrix carbon ceramic prepared by sol-gel method (SiO$_2$/C)

[n] Electroactive nanostructured films of chitosan (Ch) and nickel tetrasulfonated phtahlocyanine (NiTsPc) produced via electrostatic layer-by-layer technique on indium tin oxide (ITO) electrode

[o] Amino-group functionalized mesoporous Fe$_3$O$_4$@graphene sheets (GS)-modified glassy carbon electrode (GCE)

[p] Graphite electrode (Gr) modified with positively charged poly(diallyldimethylammonium chloride) (PDDA) and negatively charged multiwalled carbon nanotubes (MWCNTs) wrapped with polystyrene sulfonate (PSS)

[q] Nickel(II) phthalocyanine (NiPc) synthesized in situ in the pores of a carbon ceramic material (SGN)

[r] Ionic liquid (IL) *N*-butylpyridinium hexafluoro-phosphate (BPPF$_6$)-modified carbon paste electrode (CPE)

[s] Modified glassy carbon electrode (GCE) with the 1-butyl-3-methylimidazolium 2-amino-3-mercaptopropionic acid salt ionic liquid functionalized graphene composites (IL-G)

[t] Gold nanoparticles@polyaniline core–shell nanocomposites (AuNPs@PANI)-modified glassy carbon electrode

[u] Tyrosinase-immobilized on single wall carbon nanotubes polypyrrole composite (SWNT-Ppy) electrode

[v] Graphene flowers (GEF) used to modified a carbon fiber electrode (CFE)

[w] Indium tin oxide (ITO) glass electrode modified with 2,2-azino-bis(3-ethylbenzthiazoline-6-sulfonic acid) (ABTS) immobilized on carbon nanotubes (CNT)

Conclusions

In summary, an ionic silsesquioxane containing the 1,4-diazoniabicyclo[2.2.2]octane group was deposited on the surface of a mesoporous silica xerogel. Afterwards, it was performed the immobilization of CuTsPc by electrostatic interactions between de sulfonic groups of phthalocyanine and the ammonium groups of ionic silsesquioxane. The presence of the silsesquioxane on the silica surface was confirmed by infrared spectroscopy, obtained after heat treatment at 130 °C. The immobilization of CuTsPc was evidenced by UV-Vis spectroscopy, where the Si/Db/CuTsPc material showed the characteristic absorption in the Q-band region of phthalocyanine. This material was successfully employed in the construction of CPE, showing electrochemical response to dopamine redox process. The linear response of Si/Db/CuTsPc CPE was observed in the range of 0.010 to 0.107 mmol L^{-1}, at pH 4.5, under oxygen atmosphere. The achieved detection limit was 0.42 μmol L^{-1} and the sensitivity was 7.15 μA (mmol $L^{-1})^{-1}$. Therefore, the Si/Db/CuTsPc is a very promising material to be used in the development of electrochemical sensor for dopamine.

References

1. Zhang A, Neumeyer JL, Baldessarini RJ (2007) Chem Rev 107:274–302
2. Yang L, Liu D, Huang J, You T (2014) Sensors Actuators B 193:166–172
3. Qian T, Yu C, Zhou X, Wu S, Shen J (2014) Sensors Actuators B 193:759–763
4. Bouri M, Lerma-García MJ, Salghi R, Zougagh M, Ríos A (2012) Talanta 99:897–903
5. Feng J-J, Guo H, Li Y-F, Wang Y-H, Chen W-Y, Wang A-J (2013) ACS Appl Mater Interfaces 5:1226–1231
6. Syslová K, Rambousek L, Kuzma M, Najmanová V, Bubeníková-Valešová V, Slamberová R, Kačer P (2011) J Chromatogr A 1218:3382–3391
7. Mu Q, Xu H, Li Y, Ma S, Zhong X (2014) Analyst 139:93–98
8. Xue C, Han Q, Wang Y, Wu J, Wen T, Wang R, Hong J, Zhou X, Jiang H (2013) Biosens Bioelectron 49:199–203
9. Yu B, Yuan H, Yang Y-Y, Cong H-L, Hao T-Z, Xu X-D, Zhang X-L, Yang S-J, Zhang L-X (2014) Chin Chem Lett 25:523–528
10. Fu C, Yang W, Chen X, Evans DG (2009) Electrochem Commun 11:997–1000
11. Wang F, Yang J, Wu K (2009) Anal Chim Acta 638:23–28
12. Kang J, Zhuo L, Lu X, Wang X (2005) J Solid State Electrochem 9:114–120
13. Salgado R, del Rio R, del Valle MA, Armijo F (2013) J Electroanal Chem 704:130–136
14. Li NB, Ren W, Luo HQ (2008) J Solid State Electrochem 12:693–699
15. Ti C-C, Kumar SA, Chen S-M (2009) J Solid State Electrochem 13:397–406
16. Zhang L, Shi Z, Lang Q (2011) J Solid State Electrochem 15:801–809
17. Yang S, Li G, Yang R, Xia M, Qu L (2011) J Solid State Electrochem 15:1909–1918
18. Švancara I, Vytřas K, Kalcher K, Walcarius A, Wang J (2009) Electroanalysis 21:7–28
19. Ardakani MM, Talebi A, Naeimi H, Barzoky MN, Taghavinia N (2009) J Solid State Electrochem 13:1433–1440
20. Liu C, Zhang J, Yifeng E, Yue J, Chen L, Li D (2014) Electron J Biotecnol 17:183–188
21. Sanghavi BJ, Hirsch G, Karna SP, Srivastava AK (2012) Anal Chim Acta 735:37–45
22. Arenas LT, Gay DSF, Moro CC, Dias SLP, Azambuja DS, Costa TMH, Benvenutti EV, Gushikem Y (2008) Microporous Mesoporous Mater 112:273–283
23. Sing KSW, Everett DH, Haul RAW, Moscou L, Pierotti RA, Rouquérol J, Siemieniewska T (1985) Pure Appl Chem 57:603–619
24. Walcarius A, Etienne M, Bessière J (2002) Chem Mater 14:2757–2766
25. Melde BJ, Johnson BJ, Charles PT (2008) Sensors 8:5202–5228
26. Maroneze CM, Rahim A, Fattori N, Costa LP, Sigoli FA, Mazali IO, Custodio R, Gushikem Y (2014) Electrochim Acta 123:435–440
27. Walcarius A, Mandler D, Cox JA, Collinson M, Lev O (2005) J Mater Chem 15:3663–3689
28. Nunes MR, Gushikem Y, Landers R, Dupont J, Costa TMH, Benvenutti EV (2012) J Sol-Gel Sci Technol 63:258–265
29. Gushikem Y, Benvenutti EV, Kholin YV (2008) Pure Appl Chem 80:1593–1611
30. Gay DSF, Fernandes THM, Amavisca CV, Cardoso NF, Benvenutti EV, Costa TMH, Lima EC (2010) Desalination 258:128–135
31. Pereira MB, Michels AF, Gay DSF, Benvenutti EV, Costa TMH, Horowitz F (2010) Opt Mater 32:1170–1176
32. de Menezes EW, Nunes MR, Arenas LT, Dias SLP, Garcia ITS, Gushikem Y, Costa TMH, Benvenutti EV (2012) J Solid State Electrochem 16:3703–3713
33. Caldas EM, de Menezes EW, Pizzolato TM, Dias SLP, Costa TMH, Arenas LT, Benvenutti EV (2014) J Sol-Gel Sci Technol 72:282–289
34. Arenas LT, Dias SLP, Moro CC, Costa TMH, Benvenutti EV, Lucho AMS, Gushikem Y (2006) J Colloid Interface Sci 297:244–250
35. de Menezes EW, Lima EC, Royer B, de Souza FE, dos Santos BD, Gregório JR, Costa TMH, Gushikem Y, Benvenutti EV (2012) J Colloid Interface Sci 378:10–20
36. de Jesus CG, dos Santos V, Canestraro CD, Zucolotto V, Fujiwara ST, Gushikem Y, Wohnrath K, Pessoa CA (2011) J Nanosci Nanotechnol 11:1–10
37. Sorokin AB (2013) Chem Rev 113:8152–8191
38. Toma HE, Bonifácio LS, Anaissi FJ (2005) Quim Nova 28:897–900
39. Oni J, Nyokong T (2001) Anal Chim Acta 434:9–21
40. Santos LSS, Landers R, Gushikem Y (2011) Talanta 85:1213–1216
41. Gutierrez AP, Griveau S, Richard C, Pailleret A, Granados SG, Bedioui F (2009) Electroanalysis 21:2303–2310
42. Perez EF, Kubota LT, Tanaka AA, de Oliveira NG (1998) Electrochim Acta 43:1665–1673
43. Canevari TC, Luz RCS, Gushikem Y (2008) Electroanalysis 20:765–770
44. Rahim A, Barros SBA, Arenas LT, Gushikem Y (2011) Electrochim Acta 56:1256–1261
45. Barros SBA, Rahim A, Tanaka AA, Arenas LT, Landers R, Gushikem Y (2013) Electrochim Acta 87:140–147
46. Sancy M, Silva JF, Pavez J, Zagal JH (2013) J Chil Chem Soc 58:2117–2121
47. Santos WJR, Sousa AL, Sotomayor MPT, Damos FS, Tanaka SMCN, Kubota LT, Tanaka AA (2009) J Braz Chem Soc 20:1180–1187

48. Shaidarova LG, Gedmina AV, Artamonova ML, Chelnokova IA, Budnikov HC (2013) J Anal Chem 68:516–524

49. Rahim A, Barros SBA, Kubota LT, Gushikem Y (2011) Electrochim Acta 56:10116–10121

50. Arenas LT, Pinheiro AC, Ferreira JD, Livotto PR, Pereira VP, Gallas MR, Gushikem Y, Costa TMH, Benvenutti EV (2008) J Colloid Interface Sci 318:96–102

51. Pavan FA, Gobbi SA, Costa TMH, Benvenutti EV (2002) J Therm Anal Calorim 68:199–206

52. Gregg SJ, Sing KSW (1982) Adsorption, surface area and porosity, 2nd edn. Academic, London

53. Ying JY, Benziger JB, Navrotsky A (1993) J Am Ceram Soc 76: 2571–2582

54. Costa TMH, Gallas MR, Benvenutti EV, da Jornada JAH (1997) J Non-Cryst Solids 220:195–201

55. Foschiera JL, Pizzolato TM, Benvenutti EV (2001) J Braz Chem Soc 12:159–164

56. Arenas LT, Aguirre TAS, Langaro A, Gushikem Y, Benvenutti EV, Costa TMH (2003) Polymer 44:5521–5525

57. Arenas LT, Langaro A, Gushikem Y, Moro CC, Benvenutti EV, Costa TMH (2003) J Sol-Gel Sci Technol 28:51–56

58. Siqueira JR, Gasparotto LHS, Crespilho FN, Carvalho AJF, Zucolotto V, Oliveira ON (2006) J Phys Chem B 110:22690–22694

59. Leznoff CC, Lever ABP (1989) Phthalocyanines properties and applications Vol 1. John Wiley & Sons, New York

60. Machado ME, de Menezes EW, Bregles LP, Caramão EB, Benvenutti EV, Zini CA (2013) J Sep Sci 36:1636–1643

61. Malem F, Mandler D (1993) Anal Chem 65:37–41

62. Wu D, Li Y, Zhang Y, Wang P, Wei Q, Du B (2014) Electrochim Acta 116:244–249

63. Winter E, Codognoto L, Rath S (2006) Electrochim Acta 51:1282–1288

64. Alencar WS, Crespilho FN, Santos MRMC, Zucolotto V, Oliveira ON, Silva WC (2007) J Phys Chem C 111:12817–12821

65. Zecevic S, Simic-Glavaski B, Yeager E, Lever ABP, Minor PC (1985) J Electroanal Chem 196:339–358

66. Manjunatha R, Suresh GS, Melo JS, D'Souza SF, Venkatesha TV (2010) Sensors Actuators B 145:643–650

67. Santos CS, Ferreira RT, Calixto CMF, Rufino JL, Garcia JR, Fujiwara ST, Wohnrath K, Pessoa CA (2014) J Appl Electrochem 44:1047–1058

68. Shieh Y-T, Lu Y-T, Wang T-L, Yang C-H, Lin R-H (2014) J Solid State Electrochem 18:975–984

69. Zuo X, Zhang H, Li N (2012) Sensors Actuators B 161:1074–1079

70. Nyokong T (2008) J Porphyrins Phthalocyanines 12:1005–1021

71. Zhou Y, Tang W, Wang J, Zhang G, Chai S, Zhang L, Liu T (2014) Anal Methods 6:3474–3481

72. Sun W, Yang M, Jiao K (2007) Anal Bioanal Chem 389:1283–1291

73. Bard AJ, Faulkner LR (1980) Electrochemical methods fundamentals and applications. Wiley, New York

74. Laviron E (1979) J Electroanal Chem 101:19–28

75. Wang C, Xu P, Zhuo K (2014) Electroanalysis 26:191–198

76. Yang L, Liu S, Zhang Q, Li F (2012) Talanta 89:136–141

77. Min K, Yoo YJ (2009) Talanta 80:1007–1011

78. Du J, Yue R, Ren F, Yao Z, Jiang F, Yang P, Du Y (2014) Biosens Bioelectron 53:220–224

79. Chih Y-K, Yang M-C (2013) Bioelectrochemistry 91:44–51